Charging toward improved lithium-ion polymer electrolytes: exploiting synergistic experimental and computational approaches to facilitate materials design

Journal:	*Molecular Systems Design & Engineering*
Manuscript ID	ME-PER-12-2018-000105.R1
Article Type:	Perspective
Date Submitted by the Author:	29-Jan-2019

Complete List of Authors:	Ketkar, Priyanka; University of Delaware, Chemical and Biomolecular Engineering Shen, Kuan-Hsuan; The Ohio State University Hall, Lisa; The Ohio State University, Epps, III, Thomas; University of Delaware, Chemical and Biomolecular Engineering

Charging toward improved lithium-ion polymer electrolytes: exploiting synergistic experimental and computational approaches to facilitate materials design

Priyanka M. Ketkar,[a] Kuan-Hsuan Shen,[b] Lisa M. Hall,*[b] and Thomas H. Epps, III*[a,c]

[a]*Department of Chemical and Biomolecular Engineering, University of Delaware, Newark, DE 19716, USA. E-mail: thepps@udel.edu*

[b]*William G. Lowrie Department of Chemical and Biomolecular Engineering, The Ohio State University, Columbus, OH 43210, USA. Email: hall.1004@osu.edu*

[c]*Department of Materials Science and Engineering, University of Delaware, Newark, DE 19716, USA*

Design, System, and Applications

Efficient lithium-ionic conduction is a crucial property that must be improved in polymer electrolytes in order to meet the energy demands of next-generation lithium-ion battery (LiB) devices. The transport of lithium ions is dictated by concerted processes that occur at scales ranging from local ion and polymer interactions to the global thermodynamics of composite electrolyte materials. This Perspective examines how experimental and computational methods were applied synergistically to connect transport-governing phenomena across multiple size scales and unite various polymer electrolyte systems under a set of universal parameters to accelerate design efforts. Furthermore, avenues for the enhancement of experimental and computational

tools, formulation of novel materials, and incorporation of polymer electrolytes into robust LiBs are suggested.

Abstract

Ion-conducting polymer electrolytes are attractive materials for all-solid-state lithium-ion batteries (LiBs) as a result of their potential to improve performance, mitigate safety concerns, and facilitate efficient device processing. Understanding how lithium-ionic transport is influenced by the macromolecular features, such as dielectric strength, solvation site connectivity, monomer segment relaxation timescales, segregation strength, and mesophase composition, is crucial for advancing ion-conducting materials. The integration of experimental and computational efforts can provide comprehensive links between chemical and structural characteristics (e.g., ion solvation, chain mobility, morphology) and macroscopic performance properties, accelerating the adoption of next-generation polymer electrolytes. This perspective highlights several synergistic experimental-computational approaches that have provided unique insights into local ion and polymer interactions, chain dynamics, and thermodynamics to promote the rational design of new ion-conducting polymers. Additionally, this work concludes with several suggested areas in which methodologies can be augmented, novel properties can be realized, and polymer electrolytes can be integrated to generate more robust LiB systems.

1. Introduction

Lithium-ion batteries (LiBs) constitute a $30 billion dollar industry that is expected to grow almost five-fold by the year 2026 because of the ubiquity of batteries in electric vehicles, consumer electronics, and renewable energy storage devices.[1] In comparison to many other battery types for

these applications, LiBs are desirable due to their high energy density, high cycling efficiency, minimal memory effects, and low maintenance.[2, 3] However, additional developments in safety and device performance (e.g., capacity, efficiency, charging rate) are necessary to meet the growing demands of LiB consumers, and several of these developments can be achieved through the engineering of novel electrolyte systems. Shortcomings in LiB performance often preclude LiBs from some high-demand applications.[4-6] Additionally, conventional LiBs also suffer from safety concerns such as fires, material decomposition, and gas evolution that generally are a symptom of lithium dendrite growth, flammable electrolytes, and electrochemical incompatibility between the electrolyte and electrodes.[7] These current electrolyte systems, which usually are composed of lithium salts (e.g., $LiPF_6$) in organic liquid solvents (e.g., ethylene carbonate-dimethyl carbonate) in combination with a separator membrane (e.g., polyethylene or polypropylene),[7-9] have conductivities on the order of 10^{-2} S/cm at room temperature, can perform ~1000 charge/discharge cycles, and possess electrochemical stability windows between 0.8 V and 4.5 V vs. Li^+/Li.[7, 10, 11] To meet the upcoming market needs for LiBs, new electrolyte systems must transport lithium ions effectively, while also addressing the safety and performance considerations, and maintaining processibility *via* inexpensive means.

Among the various electrolyte systems that can overcome limitations of liquid- or gel-based electrolytes,[12] solid polymer electrolytes are versatile materials that boast chemical stability, mechanical resilience and flexibility, relatively low densities, and facile processibility.[13-15] Examples of several polymer electrolyte systems are provided in Fig. 1. In short, the polymer electrolyte should solvate lithium ions (the anions may be free as in a salt-doped system or immobilized as in a single-ion system[16]) and facilitate cation transport between electrodes, as depicted in the rightmost portion of Fig. 2. For example, salt-doped poly(ethylene oxide) (PEO),[17]

the archetypal polymer electrolyte, conducts lithium ions efficiently at elevated temperatures but fails to incorporate other desirable properties (e.g., adequate conductivity while maintaining significant modulus to mitigate dendrite growth) that may be challenging to achieve in a simple homopolymer system.[18] Fortunately, competing properties can be decoupled and simultaneously optimized in nanostructured block polymers (BPs), such as polystyrene-*block*-poly(ethylene oxide) (PS-*b*-PEO).[19] In PS-*b*-PEO, the self-assembled PS domains typically exhibit a high modulus below their glass transition temperature (T_g; ~100 °C), and the PEO domains exhibit good ionic solvation and conduction properties at moderate temperatures.[18] Despite favorable attributes, the crystallization of PEO at ~60 °C leads to poor room temperature conductivity in most PEO-based electrolytes.[13]

Alternative salt-doped and single-ion polymer chemistries and architectures have been employed to overcome the limitations of PEO and PS-*b*-PEO electrolytes, as well as to impart other useful properties such as reduced charge polarization and enhanced processibility.[16] Nonlinear polymer architectures such as comb polymers (e.g., poly(oligo-oxyethylene methacrylate) [POEM]),[20] bottle brush BPs,[21, 22] star-shaped BPs,[23, 24] and cross-linked polymers[25, 26] have been investigated because of the favorable ionic transport, mesophase domain size control, or electrochemical stability afforded by these systems. In lieu of complex polymer syntheses, various additives such as nanoparticles (NPs),[27, 28] ionic liquids (ILs),[29, 30] and other polymers (i.e., polymer blends)[31-34] also have offered a facile, modular route to imparting desirable materials characteristics. However, despite the developments reported across a rich breadth of polymer electrolyte systems, these macromolecule-based electrolytes still have at least a couple orders of magnitude lower ionic conductivities than their liquid-state counterparts.[16] Thus, realizing the

unique advantages of polymer electrolytes, such as flexibility and processibility, requires significant improvements in polymer electrolyte technology.

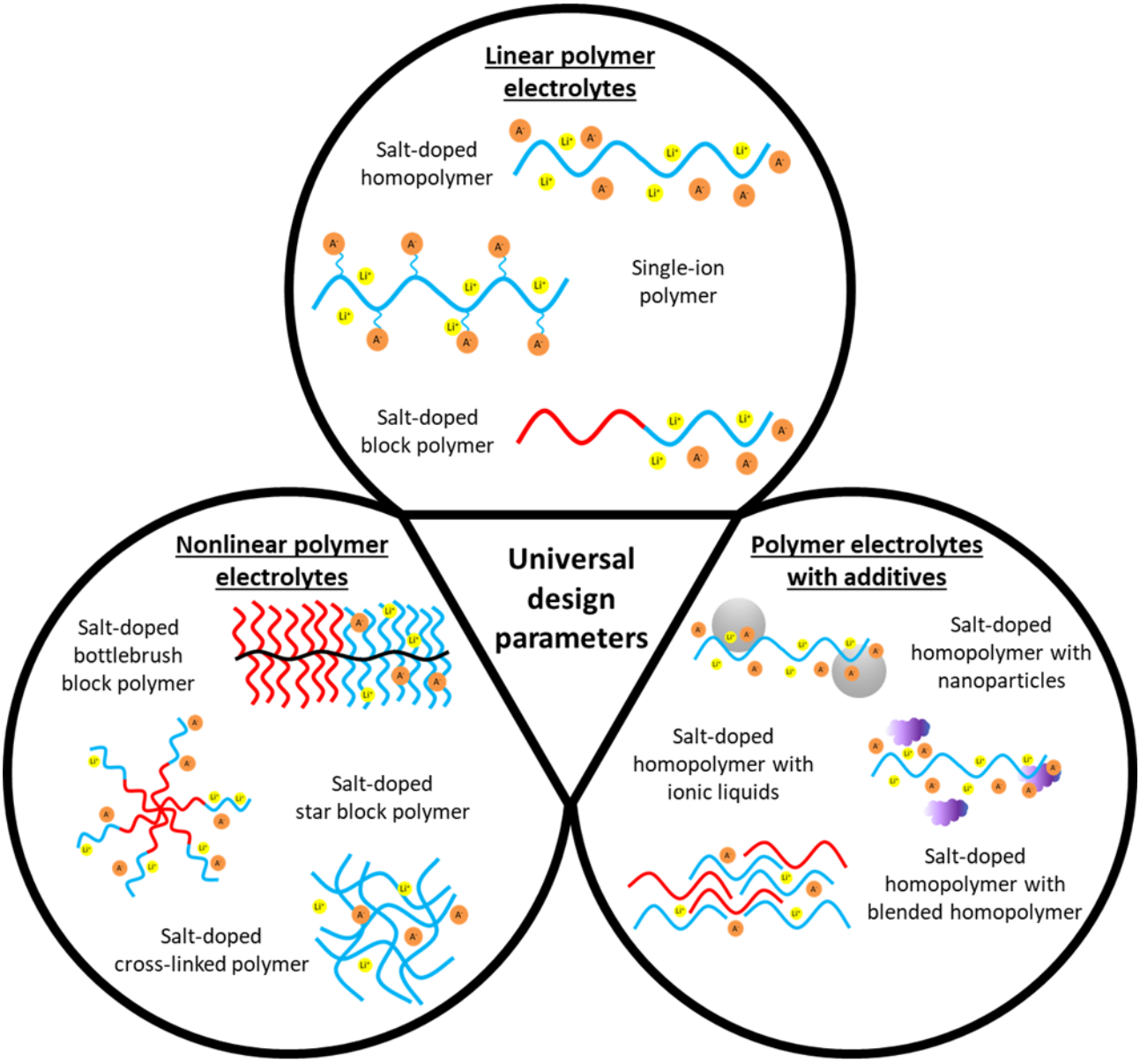

Fig. 1. Summary of several polymer systems that have been studied as electrolytes. The chemistry, architecture, and additive content of the electrolytes can be tuned to impart beneficial properties, such as high ionic conductivity, high electrochemical stability, and enhanced processibility. The development of a universal design model that accounts for the characteristics of diverse electrolyte systems can promote the efficient design of novel electrolytes.

Consolidating the knowledge of various polymer electrolyte systems to a set of universal parameters and understanding the independent and synergistic effects of these parameters on the macroscopic electrolyte properties can unlock more systematic approaches to polymer electrolyte design. The integration of experimental and computational efforts presents an effective strategy to link these parameters (e.g., dielectric strength, solvation site connectivity, monomer segment relaxation timescales, segregation strength, and mesophase composition) to both synthetic variables and material properties. Computational studies provide both qualitative and quantitative explanations to guide experimental investigations and support the key results/conclusions, and experimental data allow computational methods and assumptions to be validated such that those methods can be extended to facilitate the rapid discovery of new phenomena. The synergistic analyses discussed in this Perspective have advanced our knowledge and ability to control phenomena across multiple length scales, such as local ion and polymer interactions, chain dynamics, and thermodynamics (Fig. 2). Future advances in polymer electrolyte technology will require the integration current knowledge to develop novel materials and the connection of larger-scale phenomena, such as electrode-electrolyte interactions, to effects on smaller-scale electrolyte behavior.

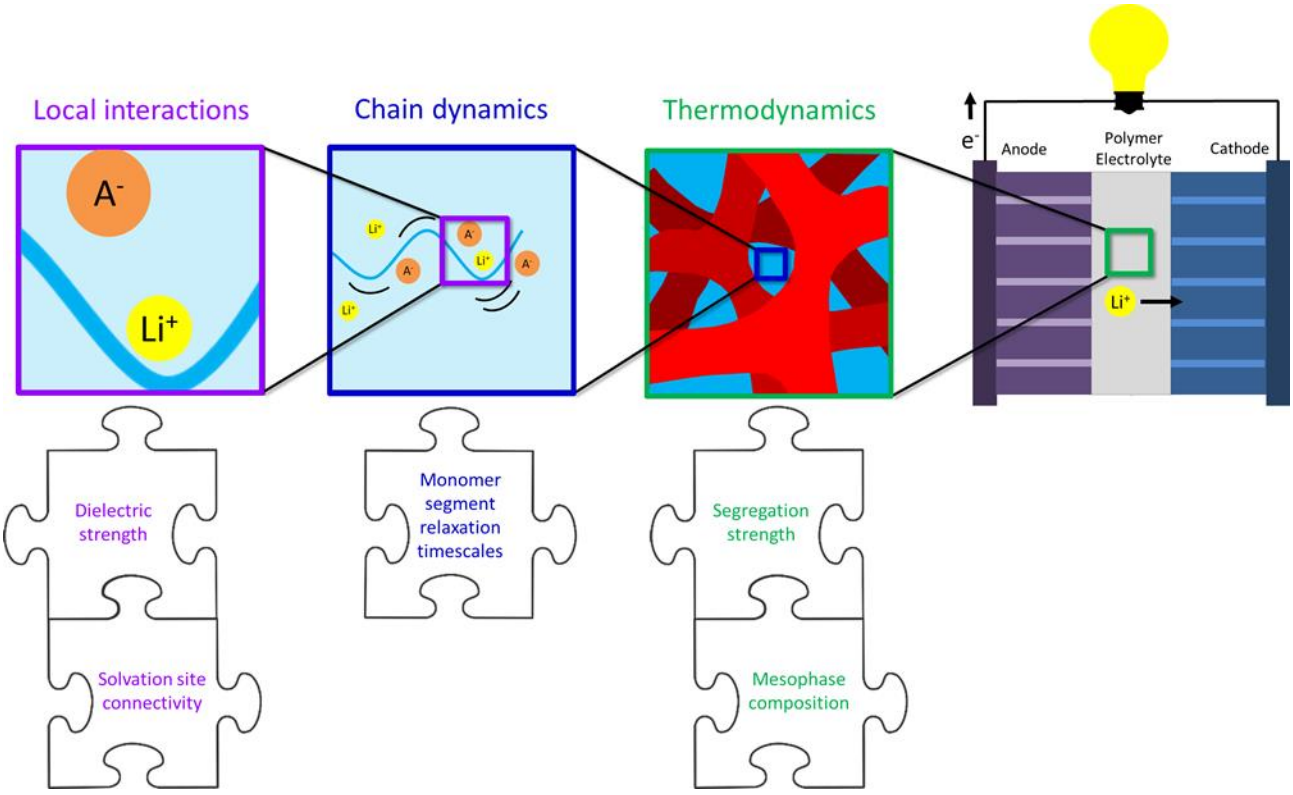

Fig. 2. Outline of several polymer electrolyte key parameters discussed in this Perspective.

2. Local ion-ion and ion-polymer interactions

Lithium-ion redox reactions at the electrodes are essential to the energy generation and storage processes in LiBs. Polymer electrolytes must solvate and assist the transport of lithium ions between the electrodes as efficiently as possible to facilitate these reactions. Ion solvation (i.e., the interruption of cation-anion codiffusion) is crucial because the transport of anions and neutral ion clusters (i.e., pairs and larger aggregates) does not readily contribute to energy generation and storage. Typically, the fraction of free lithium ions is maximized through strong interactions between the host polymer and lithium ions (Fig. 3a), and the segmental motion of the

polymer chains, which often is correlated to the T_g of the conductive polymer, moderates lithium-ion diffusion. An abundant concentration of sites on the polymer chains that interact favorably with lithium ions ensures continued lithium-ion solvation and can enable transport between the two electrodes (Fig. 3b). Because the nature of these local interactions can be difficult to probe accurately *via* experimental techniques, computational tools can aid in the design of effective polymer electrolyte hosts that maximize the energy capacity of LiBs. Computational studies have focused on ion transport in polymer electrolytes at various levels of chemical detail and computational expense.[35] Although a quantum description of local ion coordination in polymer electrolytes (i.e., *ab initio* calculations) can allow the study of charge transfer without empirical interaction potentials, the applications of quantum models are usually limited due to large computational costs.[35] Nevertheless, some quantum mechanical calculations can be applied during molecular dynamics (MD) simulations: for example, Car-Parrinello or similar techniques have been applied to facilitate a detailed description of local ion transport mechanisms.[36] In this Perspective, we focus on classical simulations with empirical potentials or force fields developed with quantum mechanical calculations (i.e., the calculation of equilibrium charge distribution by density functional theory (DFT) to determine parameterized potentials).[37-39] These classical simulations can describe ion coordination while accessing the longer timescales relevant to the polymer dynamics of interest. Moreover, with specialized methodology, ion solvation and the mechanisms of ion hopping can be analyzed in detail.[40]

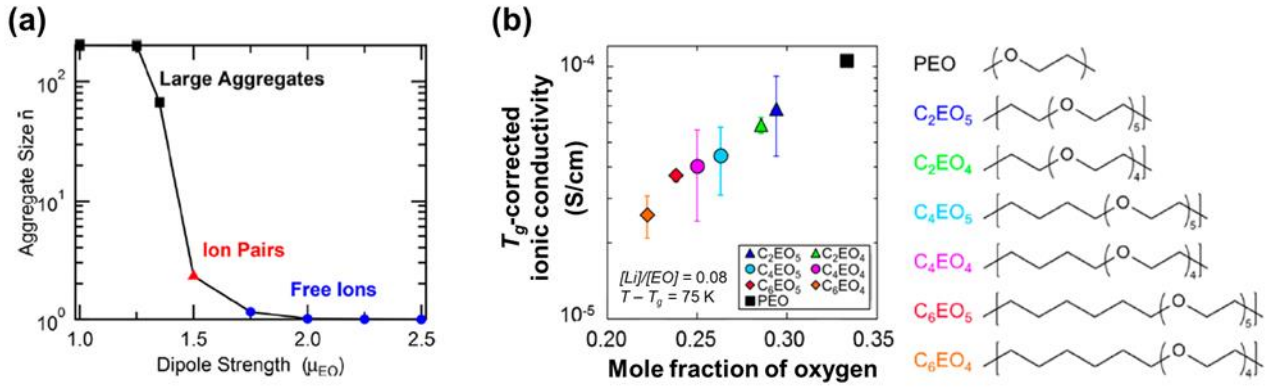

Fig. 3. (a) The effect of dielectric constant (dipole strength) on the size of ion aggregates in coarse-grained MD simulations of polymer electrolyte systems. Image was adapted with permission from ref. 41. Copyright 2018 American Chemical Society. (b) T_g-corrected ionic conductivity of various salt-doped polyethers in which the effect of solvation site concentration on the ionic conductivity is visible. Images were adapted with permission from ref. 42. Copyright 2016 American Chemical Society.

Lithium-ion solvation is facilitated when the polymer host has a sufficiently large dielectric strength, such that the ion solvation energy is favorable in comparison to the lattice energy of the cation and anion. For example, the ionic conductivity of various lithium bis(trifluoromethane)sulfonimide (LiTFSI)-doped poly(glycidyl ether) species, measured *via* electrochemical impedance spectroscopy (EIS) at 100 °C, increased monotonically with increasing dielectric constant of the host polymer irrespective of T_g (i.e., the degree of chain mobility, proxied by the difference between the operating temperature and T_g, was not the dominant mechanism that dictated the ionic conductivity).[43] These qualitative dielectric constant and ion diffusivity trends from the EIS experiments were captured *via* atomistic MD simulations and revealed that the codiffusion of the cations and anions decreased with increasing host polymer dielectric constant.[43]

This reduction in ionic codiffusion was thought to be promoted by stronger polymer-cation interactions that electrostatically screened cation-anion interactions.[43] The high ionic conductivities measured at increased dielectric constants were attributed to the electrolytes approaching the Nernst-Einstein limit, in which cation and anion codiffusion is negligible, and the ionic conductivity is predicted accurately from the pure ionic diffusivities.[43] It has been suggested that the lithium-ion transference (the portion of the ionic conductivity that is contributed by lithium-ion motion) also could be greater in high dielectric systems in which lithium ions are solvated strongly.[44]

An alternative method to increase the lithium-ion transference number employs the incorporation of single-ion monomer segments that tether the anion to polymer chains to limit anion mobility. In these single-ion systems, it is especially crucial to maximize lithium-ion solvation so that lithium-ion transport is not limited by interactions with the immobile anions.[45] The effects of cation-anion binding on ionic conductivity were studied experimentally in cross-linked single-ion [(poly(ethylene glycol) diacrylate)-*co*-(4-styrenesulfonlyl) (trifluoromethanesulfonyl)imide] (PEGDA-*co*-STFSI) copolymers by the Schaefer group.[46] Varying the cations (Li^+, Na^+, K^+, Mg^{2+}, Ca^{2+}, and Al^{3+}) significantly altered the ionic conductivity at 25 °C (Fig. 4a) with lithium-ion-containing electrolytes having the highest conductivity of ~10^{-7} S/cm and calcium-ion-containing electrolytes having the lowest conductivity of ~10^{-10} S/cm.[46] Although DFT calculations of the cation-STFSI binding energies (Fig. 4b) and Raman spectroscopy measurements of unbound (i.e., not bound to cations) STFSI anion concentration (Fig. 4c) suggested similar qualitative trends with respect to ionic conductivity, the overall differences in unbound STFSI concentration across cation samples were insignificant in comparison to the range of ionic conductivities.[46] The authors speculated that the discrepancy

between the unbound STFSI concentration and conductivity data may be the result of undetermined charged complexes that were expected to have lower binding energies and contribute to the conductivity in a different manner from unbound ions or neutral ion clusters.[46] Similar charged complexes also were found in MD simulations of a LiTFSI-doped PEO-like system, in which negatively charged cation-anion complexes not only hindered lithium-ion mobility but also resulted in experimental measurements of negative transference numbers.[47-51] The difficulty in experimental characterization of the size and composition of ionic clusters, beyond free and paired ions, presents challenges in the development of systems that target the solvation of these clusters.[52] Thus, computational tools can be leveraged to augment the knowledge gained from experimental systems focused on the size scale of ion-polymer and ion-ion interactions.

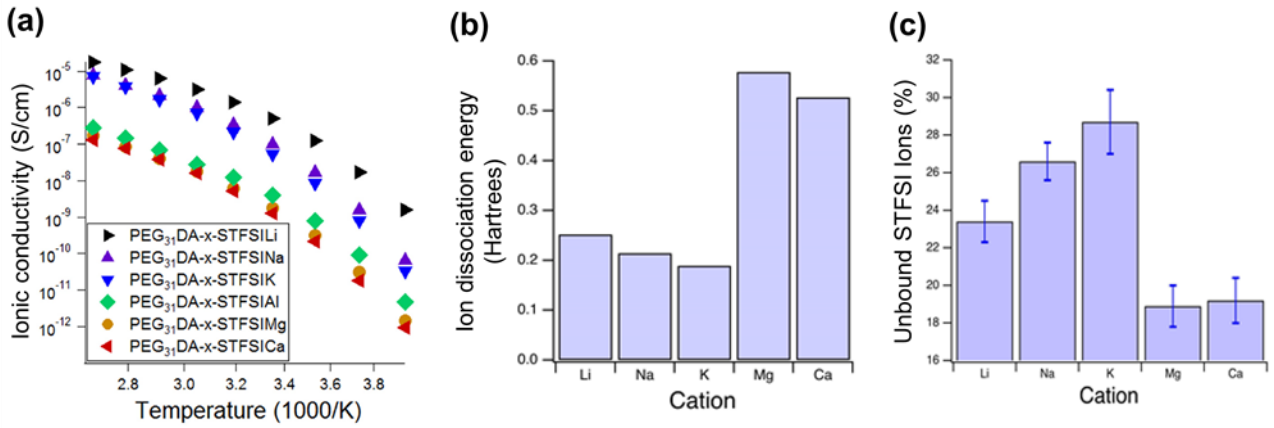

Fig. 4. The cation-dependent (a) ionic conductivities, (b) ion dissociation energies calculated by DFT, and (c) percentage of STFSI moieties not bound to cations, from Raman spectroscopy, in cross-linked PEGDA-STFSI electrolytes with 31 ethylene glycol repeat units per crosslinker (PEG_{31}DA-x-STFSI). The cations examined in this study were Li^+, Na^+, K^+, Mg^{2+}, Ca^{2+}, and Al^{3+}. Images were adapted from ref. 46.

Efficient lithium-ion transport between electrodes requires polymer electrolyte materials to form pathways in which lithium-ion solvation site connectivity is uninterrupted.[42, 53, 54] From a computational characterization standpoint, Webb et al. defined a solvation site as the centroid of five or more ether oxygens within a 3.7 Å radius, and two solvation sites were considered connected if they were closer than 3 Å to each other.[53] According to MD simulations, PEO electrolytes possessed 10-100 times more connections in solvation sites relative to polyester-based electrolytes (see Fig. 5) and followed a similar increase in ionic conductivity even after accounting for T_g effects.[53] In a follow-up study, poly(diethylene oxide-*alt*-oxymethylene) (P(2EO-MO)) exhibited a two-fold increase in solvation site connectivity and lithium-ion transference in comparison to PEO.[54] Thus, lithium-ion transference may be independently tuned through the solvation site connectivity, even if each site had a similar dielectric interaction with the ions, such as in the case of P(2EO-MO) vs. PEO. With accurate computational algorithms that can predict the solvation site connectivity, a crucial parameter that has significant implications for lithium-ionic conductivity, monomer chemistries and polymer architectures can be screened rapidly to guide experimental system choices.

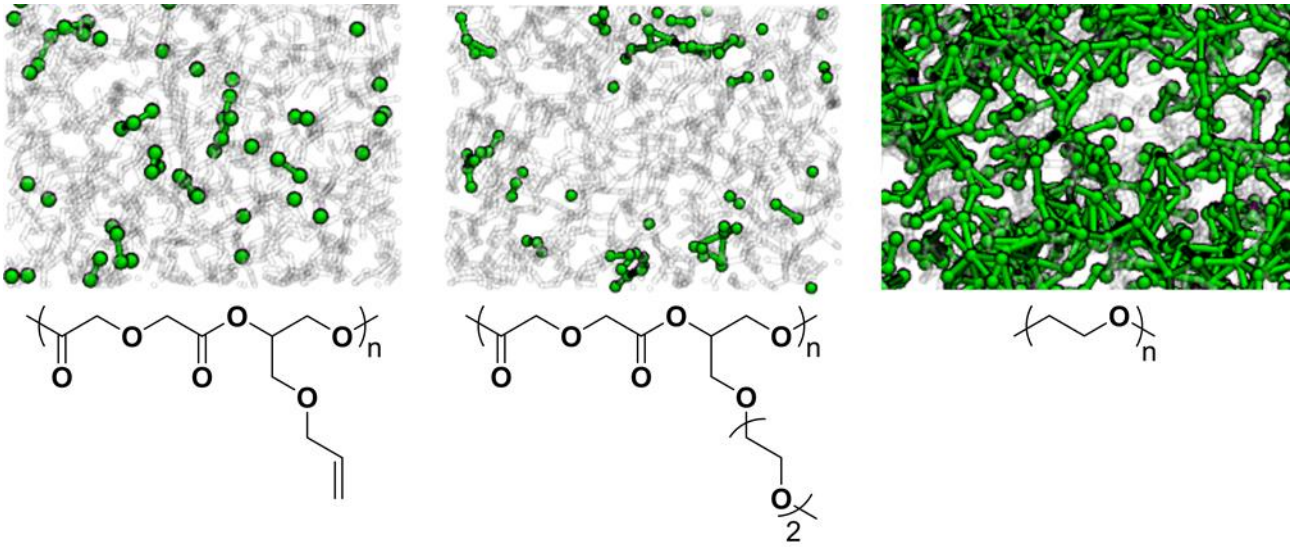

Fig. 5. A depiction of the solvation site connectivity for different polymer chemistries with the green spheres representing solvation sites and green lines representing connections between solvation sites. Images were adapted with permission from ref. 53 (https://pubs.acs.org/doi/abs/10.1021/acscentsci.5b00195). Further permissions related to the material excerpted should be directed to the American Chemical Society.

The rapid screening of electrolyte designs with respect to their solvation site connectivity and dielectric strength can be aided through improvements in experimental and computational tools. The ability to discern the size and composition of ion clusters by experimental means can allow simulated ion cluster analyses to be validated, such that the dielectric strength can be tuned to target the solvation of specific cluster sizes. The characterization of cation transference can be honed on both experimental[44] and computational fronts to formulate dielectric systems that selectively assist lithium-ion transport. Lithium-ion transference can be improved through the adaption of the Lewis-acidity (and hence dielectric interactions) of polymer hosts to foster stronger anion-polymer complexation than cation-polymer complexation.[55, 56] Interestingly, Park and coworkers significantly improved lithium-ionic conduction in LiTFSI-doped PS-*b*-PEO through the implementation of end-groups (less than 1 mol% of the PEO domains) that exhibited hydrogen

bonding interactions with the anions.[57] These pseudo-single-ion materials[16] may achieve higher transference numbers than traditional LiTFSI-doped PEO electrolytes (~0.2)[57] without the synthetic complexity of traditional single-ion systems, in which the polymers bear an explicit charge. On the other hand, the concept of solvation site connectivity can be exploited to place single-ion and lithium-ion solvation functionalities in close proximity or even to develop monomers that contain both functionalities[16] to aid lithium-ion dissociation and transport in single-ion systems. Beyond solvation, the mobility of ions *via* polymeric chain motion should be examined to produce electrolytes with superior lithium-ionic conductivity.

3. Polymer electrolyte chain dynamics

Although the maximization of ion solvation increased the availability of free cations and improved conductivity in many cases (Fig. 3), other factors were equally critical to charge transport. For example, the variation of cation solvation or cation identity did not affect the ionic conductivity of linear PEO-based single-ion electrolytes examined by Maranas and coworkers; instead T_g was the determining factor.[58-61] This result suggests that local ion dynamics alone cannot explain the full phenomenon of lithium-ion transport. Wheatle et al. demonstrated, through coarse-grained MD simulations of salt-doped polymer electrolytes with variable dielectric constant (Fig. 6a, Fig. 6b, and Fig. 3a), that although increasing the dielectric constant of the host polymer promoted ionic conductivity in low-dielectric-constant systems (by decreasing ion aggregation, as depicted in Fig. 3a), stronger ion and polymer interactions also hindered segmental dynamics in high-dielectric-strength systems (Fig. 6b), though the presence of ions also plasticized the system.[41] The optimal ionic conductivity was achieved at an intermediate ion-polymer interaction strength at which ions were sufficiently solvated, but segmental dynamics were impaired

minimally.[41] Similar competing effects were isolated in a systematic experiment that used a series of polyethers with varying concentrations of ether groups (at a constant salt loading), as shown in Fig. 6c, Fig. 6d, and Fig. 3b.[42] Increased ether group concentrations resulted in higher solvation site connectivities and higher overall dielectric strength; however, the associated polar interactions reduced segmental motion (increased T_g, as demonstrated in Fig. 6d).[42] A clear trend of the conductivity enhancement with respect to solvation site concentration was obtained after T_g effects were corrected (Fig. 3b).[42] The deconvolution of the dielectric contributions from the host polymer and the ions can enable the ionic conductivity to be modulated.

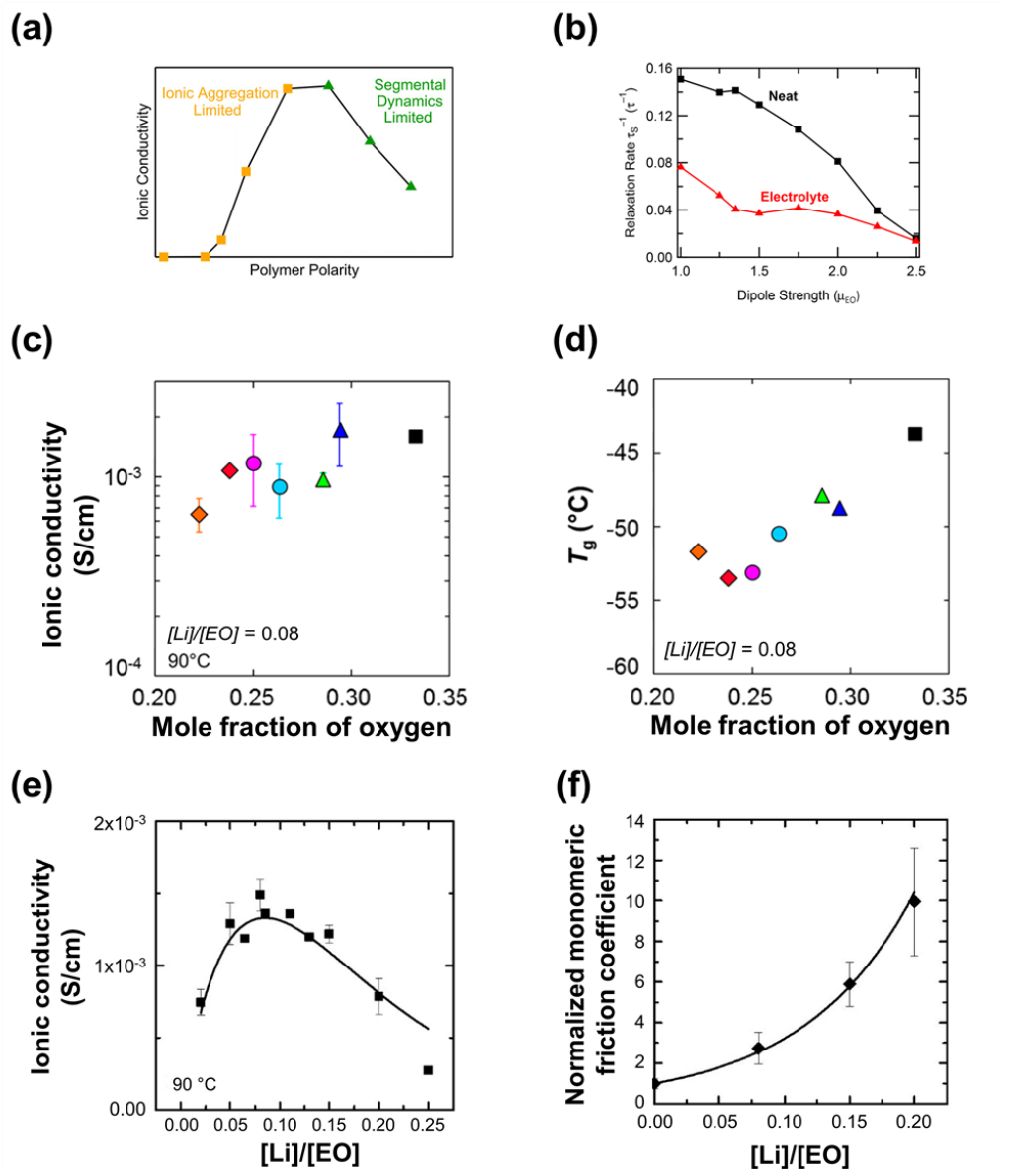

Fig. 6. Summary of the effect of dielectric ion and polymer interactions on the ionic conductivities ((a), (c), and (e)) and chain dynamics ((b), (d), and (f)) of various polymer systems. In coarse-grained MD simulations of polymer electrolyte systems ((a) and (b)), the overall dielectric constant of the host polymer (dipole strength or polymer polarity) was varied, and its effects on (a) the ionic conductivity and (b) segmental relaxation rate were probed. In a series of polyethers ((c) and (d)), the mole fraction of oxygen atoms per chain segment was varied to tune the overall dielectric strength of the polymer. (d) Ionic conductivity (at 90 °C) and (e) T_g of these polymers were measured. In PEO with varying concentrations of LiTFSI ((e) and (f)), the (e) conductivity was measured along with the (f) normalized monomeric friction coefficient, obtained from QENS measurements, which quantified the extent to which segmental motion was slowed by the salt content. Images in (a) and (b) were adapted with permission from ref. 41. Copyright 2018 American Chemical Society. Images in (c) and (d) were adapted with permission from ref. 42. Copyright 2016 American Chemical Society. Images in (e) and (f) were adapted with permission from ref. 62. Copyright 2018 American Chemical Society.

The addition of ions into a polymer electrolyte attenuates chain motion as a consequence of the dielectric ion-polymer interactions (although ion aggregation increases with ion concentration,[63] in contrast to the decrease in aggregation with host polymer dielectric strength), and this effect must be quantified. In a recent investigation of LiTFSI-doped PEO, Mongcopa et al. reported that although the ionic conductivity peaked at an intermediate salt concentration (Fig. 6e), the segmental dynamics exhibited a clear monotonic decline.[62] The segmental dynamics results, obtained by fitting quasi-elastic neutron scattering (QENS) data with a Rouse model and extracting monomeric friction coefficients (Fig. 6f),[62] suggested that at LiTFSI concentrations of 12.5 ethylene oxide moieties per lithium ion ([EO]:[Li] = 12.5 or [Li]/[EO] = 0.08) or higher, the significant decline in chain motion outweighed the effect of increasing lithium-ion concentration on ionic conductivity. This nonmonotonic trend in ionic conductivity was captured qualitatively through a model that accounted for Rouse dynamics and charge carrier concentration;[62] however, this basic Rouse model did not describe the effects of lithium-ion subdiffusion and polymer relaxation times across all length scales simultaneously.[64] Webb et al. developed a modified Rouse model that incorporated ion-polymer and ion-ion interactions, and this adjusted model suggested that the global friction contribution from ion-ion interactions had a significant effect on segmental dynamics.[64] Altogether, the effects of ion concentration, host polymer dielectric strength, and solvation site connectivity on the free lithium-ion concentration and segmental dynamics are intrinsically, and sometimes inversely, linked. As such, other variables must be investigated to improve segmental dynamics, so as to not compromise the availability of free lithium-ions.

In lieu of modifying dielectric variables, the chain length can be adjusted to enhance segmental motion. Although the ionic conductivity of LiTFSI-doped PEO homopolymer

electrolytes decreased with molecular weight up to 1 kg/mol,[65] the opposite trend was reported for LiTFSI-doped PS-*b*-PEO BPs up to 100 kg/mol.[66] According to coarse-grained MD simulations performed by Ganesan et al., cation diffusion in homopolymers was influenced only by the molecular-weight-dependent chain dynamics.[56] In BPs, however, cation transport was limited by ion solvation at the interfaces between the conductive and nonconductive mesophases, and increasing the molecular weight of the BP decreased the relative volume of the low-solvation interfacial region.[56] Thus, the mechanism for ion transport was altered when one of the chain ends was tethered to a mesophase interface. A similar trend was reported in cross-linked, single-ion, PEGDA-based electrolytes when crosslinker lengths were increased.[46] One counterintuitive difference was that the addition of brush-like PEO side chains to the cross-linked framework minimally improved conductivity (by less than an order of magnitude) or even worsened conductivity in some cases.[46] The effects of tethering on chain dynamics can be further understood if the local segmental motion is probed. Sethuraman et al. demonstrated that the mobility of a simulated rubbery polymer segment increased with distance from a glassy interface to which the segment was tethered,[67] signifying that the global conductivity or average T_g may not characterize the chain dynamics accurately. Hence, it may be necessary to probe local chain mobility profiles experimentally through dynamic mechanical analysis, amplitude-modulated atomic force microscopy, solid state nuclear magnetic resonance spectroscopy, and fluorescence measurements of marker monomers.[68-70]

The characterization of local chain dynamics also should be extended to additive systems that may contain similar inhomogeneities in the electrolyte behavior, as the incorporation of components, such as ILs and NPs, is another route to increase chain motion. IL additives have been studied extensively in polymer electrolyte systems, as they are known to enhance ionic

conductivity and are considered nonflammable alternatives to traditional liquid-state electrolytes.[29, 30] Raman spectroscopy measurements of LiTFSI-doped PEO with an IL, N-methyl-N-butyl-pyrrolidiniumbis(trifluoromethane-sulfonyl)imide, indicated that addition of the IL reduced the interactions between lithium ions and the ether oxygens in PEO, although an obvious mechanism for the effects of these interactions on lithium-ion transport was not apparent.[71] MD simulations of a similar system with a Rouse-based cation transport model revealed that nearly all of the lithium ions were coordinated by ether oxygens from PEO chains and eliminated the possibility of direct lithium-ion transport *via* the IL.[36] The addition of IL to the simulated system significantly reduced the timescale of Rouse dynamics but negligibly altered the timescales of inter-chain and intra-chain hopping.[36] These results suggested that the IL plasticized the PEO chains,[36] and the decreased lithium-ion-PEO interactions, as gleaned from the Raman spectroscopy results, likely reflected faster lithium-ion transport as a result of the plasticization.

Unlike ILs, NPs do not exhibit universal mechanisms for segmental dynamics alteration.[28] Ahn et al. reported that the crystallization of $LiCF_3SO_3$-, $LiClO_4$-, and $LiPF_6$-doped PEO was interrupted (and hence, the room-temperature chain mobility was improved) through the addition of TiO_2, SiO_2, and Al_2O_3 NPs.[72] The reduction of the micrometer-scale NP sizes by ~100 times, while total NP mass was held constant, further improved the room temperature conductivity by up to an order of magnitude,[72] most likely as a result of the increased NP surface area. Additionally, the acidification of Al_2O_3 NP surfaces by the Maranas group increased the ionic conductivity of $LiClO_4$-doped PEO by up to three times in comparison to neutral Al_2O_3 NPs, but in this case, the authors proposed that acidic NPs stabilized crystalline polymer-salt regions instead of interrupting them.[73] The acidic Al_2O_3 NPs also reduced the segmental relaxation of neat PEO by a factor of approximately two and had a negligible effect on the segmental motion of the salt-doped PEO,

confirming that plasticization did not occur.[73] The PEO-salt crystal stabilization mechanism may be the result of preferential ion-NP interactions, as suggested by simulations of $LiBF_4$-doped PEO with added Al_2O_3 or TiO_2 NPs. However, in the simulated case, these interactions also decreased the mobility of amorphous PEO chains near the NP surfaces.[74, 75] A composite electrolyte system consisting of crystalline and amorphous regions may maximize lithium-ion transport[76]; high-dielectric-strength crystalline regions can drive lithium-ion solvation, and low-dielectric-strength amorphous regions can assist lithium-ion transport through superior chain mobility.

The relationship between local ion solvation and larger-scale chain dynamics must be understood such that both aspects can be tuned to maximize lithium-ion transport. Although increased dielectric strength often reduces segmental dynamics, other factors, such as the chain length and additive content, can improve chain mobility without sacrificing ion solvation. The development of tools that can probe local heterogeneities in polymer mobility will provide a more accurate representation of chain dynamics, such that improvements to regions of low mobility can be targeted in future electrolyte designs. One avenue for segmental dynamics enhancement, as mentioned earlier, involves the reduction of polymer-cation interactions,[55, 56, 77] but it is a challenge, in practice, to design systems with weak cation-polymer interactions that sufficiently solvate the cations. One solution is that ion solvation in lower-dielectric-strength polymer hosts can be enhanced through the use of novel lithium salt or single-ion monomer chemistries with lower lattice energies. Additionally, polymer hosts with higher solvation site connectivity, but lower dielectric strength per solvation site, may reduce the binding interactions that hinder lithium-ion diffusion and segmental motion. These high-conductivity materials then can be

incorporated into electrolyte systems that not only transport lithium-ions rapidly but also promote overall LiB stability and longevity.

4. Polymer electrolyte thermodynamics

Although ion-conducting homopolymers are tailored to promote efficient lithium-ion transport, longer-term LiB performance often is limited by mechanical and electrical stresses from lithium dendrites, electrochemical degradation, and delamination from the electrodes.[7, 78] To generate robust LiBs that can overcome these impediments, there is considerable interest in nanocomposite electrolytes, such as self-assembled BPs, in which properties that are often mutually exclusive in most homopolymer electrolytes (e.g., high ionic conductivity and high modulus) can be optimized separately in distinct mesophases. However, on a local scale, the presence of interfaces between these mesophases can cause inhomogeneities in dielectric interactions and segmental dynamics, while on a larger scale, the arrangement of theses mesophases can impact long-range lithium-ion transport. The investigation of the thermodynamic behavior of these complex, multicomponent electrolyte systems can guide the modulation of lithium-ion transport.

The thermodynamic behavior of polymer systems with unlike components primarily is described by the segregation strength (χN); the Flory-Huggins χ-parameter quantifies the chemical incompatibility of different species, and N represents the degree of polymerization.[79-81] As the segregation strength increases in linear diblock copolymers, the polymer chains stretch, the interfacial widths between mesophases shrink, and the order-disorder transition temperatures (T_{ODT}'s) increase (i.e., processibility is reduced).[82] However, in low-χ bottlebrush triblock terpolymers, the emergence of domains with mixed monomer segments caused the domain spacing

to increase with decreasing chain length (and hence, decreasing segregation strength),[83, 84] and this trend may allow both ionic conductivity and processibility to be improved. Ionic conductivity and processibility (lower effective interaction parameter, χ_{eff}) also were improved simultaneously in PS-*b*-POEM normal-tapered BP systems (i.e., polymers with a gradient copolymer region located between homogeneous PS and POEM blocks), in which the interfacial manipulation of the polymer chains reduced the T_g of the POEM block.[20, 85] The effects of the tapered BP architecture (and consequently, the adjustment of χ_{eff}) on the chain dynamics can be elucidated further through the local mobility measurements discussed in the previous section. Conversely, segregation strength can serve as a proxy for local segmental dynamics and can be connected across computational and experimental platforms. The χ-parameter can be estimated from the monomers' pairwise interactions in a straightforward manner *via* coarse-grained modeling, though there has been a recent push towards more detailed analyses such as renormalized one-loop (ROL) theory[86, 87] and thermodynamics integration[88] to allow a close-to-exact mapping of χ across different types of models. In experimental work, χ can be estimated by fitting a measured structure factor to a random phase approximation (RPA) model[85] or by fitting the domain spacings and interfacial widths of mesophases to a segregation strength model.[89] Although these models accurately describe the thermodynamics of neat polymer systems, further work in the modeling of ion and polymer interactions is required to properly apply these thermodynamic concepts to ion-containing polymer electrolytes.

To retain a thermodynamic framework that is similar to that employed for neat BPs, prior studies have consolidated the thermodynamics of salt-doped BPs *via* the effective Flory-Huggins parameter χ_{eff}.[63, 90] In experimental work with salt-doped PS-*b*-PEO and PS-*b*-POEM, χ_{eff} increased linearly with salt loading at low salt concentrations ($\chi_{eff} = \chi + m([Li]/[EO])$, with the

slope, *m*, quantifying the effect of the salt on the thermodynamic compatibility of the polymers and salts)[90, 91] and then plateaued to a constant value at higher salt concentrations.[89] The chemical nature of the salt anion, such as its size and Lewis acidity, dictated *m* in the linear regime and the maximum χ_{eff} in the plateau regime.[63, 89, 90] These results imply that χ_{eff} may be dependent on a combination of ion and polymer interactions, which requires further investigation.

The mechanisms behind the behavior of χ_{eff} with respect to ion concentration were explored computationally. An effort including the Wang and Balsara groups captured the linear regime of χ_{eff} through a self-consistent field theory (SCFT) approach that described cation solvation with a Born solvation energy term, which describes the energy of ion insertion into a dielectric medium; the cations were reversibly bound to a PEO-like polymer backbone to explicitly represent the complexation of lithium-ions by the ether oxygens.[63] The Born solvation energy was predicted to dictate the phase behavior of ion-containing BPs under the assumption that ion pairing was not significant at low enough salt content ([EO]:[Li] > 10, [Li]/[EO] < 0.1).[63] To explain the nonlinear behavior of χ_{eff} at higher salt concentrations, Chu et al. simulated salt-doped PS-*b*-PEO with explicit electrostatic interactions (as opposed to an overall Born solvation energy) in a heterogeneous dielectric medium.[92] They reported that the addition of salt resulted in an asymmetric phase diagram, which supported the hypothesis of a nonlinear relationship between χ_{eff} and salt loading.[92] The Hall group proposed a coarse-grained model with strong ion-polymer pairwise interactions to describe the solvation energy and implemented the model in fluids density functional theory (fDFT) and MD simulations.[93] This model qualitatively reproduced the linear and plateau regimes of χ_{eff} (and the associated increases in domain spacing) from experiments when ion-ion interactions also were included.[93] Sethuraman et al. sought to analyze the chemical origins of this behavior *via* multiscale atomistic simulations of $LiPF_6$-doped PS-*b*-PEO, but in

contrast to experimental results,[89, 94] they reported that the domain spacing of the material decreased at high salt concentrations and that the PS domain contained a substantial concentration of ions.[39] The discrepancy between the coarse-grained and atomistic characterizations may be mitigated if the dielectric effects of the polymer host, cation, and anion can be deconvoluted to more accurately represent how ions influence segregation strength.

Although the presence of ions influences the segregation strength, the segregation strength of a polymer system conversely can influence ion solvation. Gomez et al. found, *via* energy-filtered transmission electron microscopy (EFTEM), that LiTFSI was concentrated disproportionately near the centers of the PEO domains in PS-*b*-PEO (Fig. 7a), and this localization increased with PS-*b*-PEO molecular weight (and hence, segregation strength). For example, examination of a 32 kg/mol PS-*b*-PEO with a domain spacing of 16 nm showed that the lithium ions resided in the middle 63% of the PEO domain, while study of a 172 kg/mol PS-*b*-PEO with a 53 nm domain spacing suggested that lithium ions occupied the middle 34% of the PEO domain.[95] These non-uniform ion distributions were related to the local stresses within the PEO domain, as calculated by SCFT, which grew larger with closer proximity to a domain interface and with increasing molecular weight.[95] Complementary MD simulations revealed that the coordination of lithium ions with the PEO chains was weakened when these stresses increased, resulting in a reduced ion solvation.[95] Although a single LiTFSI loading of [EO]:[Li] = 12:1 was tested, and EFTEM had a minimum detection limit of [EO]:[Li] = 25:1,[95] the agreement between EFTEM and SCFT on the degree of lithium-ion localization suggests that the segregation strength can be leveraged to tune ion distributions. However, further comparison to ion distributions in other polymer electrolyte systems is necessary to understand how the segregation strength (and hence, ion distribution) can be altered quantitatively.

The exploration of stress-dependent lithium-ion solvation can be refined by the investigation of electrolyte systems in which the stress heterogeneities may differ from those of PS-*b*-PEO. For an alternative polymer ion-conductor, PS-*b*-POEM, the Epps group reported that the composition of lithium salt was directly proportional to ethylene oxide content throughout the entire POEM domain, as determined by X-ray photoelectron spectroscopy depth profiling (Fig. 7b) and neutron reflectometry (Fig. 7c).[89, 94] The discrepancy between localized salt distributions in PS-*b*-PEO and proportional salt distributions in PS-*b*-POEM may be the result of thermodynamic/segment architecture differences between PS-*b*-PEO and PS-*b*-POEM or inherent differences between the characterization techniques. Results from experimental studies revealed that salt-doped PS-*b*-PEO systems possessed χ_{eff} values between 0.1 and 0.8,[96] whereas salt-doped PS-*b*-POEM possessed χ_{eff} values between 0.1 and 0.14.[89] It is possible that the segregation strength in PS-*b*-POEM systems is sufficiently low, such that salt localization is negligible. Moreover, the branched architecture of POEM may allow the side chains to retain the flexibility necessary for lithium-ion solvation even if the backbone experiences local stresses at the interface between PS and POEM mesophases. A conclusive explanation for the difference between PS-*b*-PEO and PS-*b*-POEM electrolytes may be achieved through comprehensive comparisons between the two systems, in which a common characterization technique is used to probe the salt distributions at various salt concentrations. The experiments could be supplemented by theoretical analyses of architecture-dependent stresses at various segregation strengths.

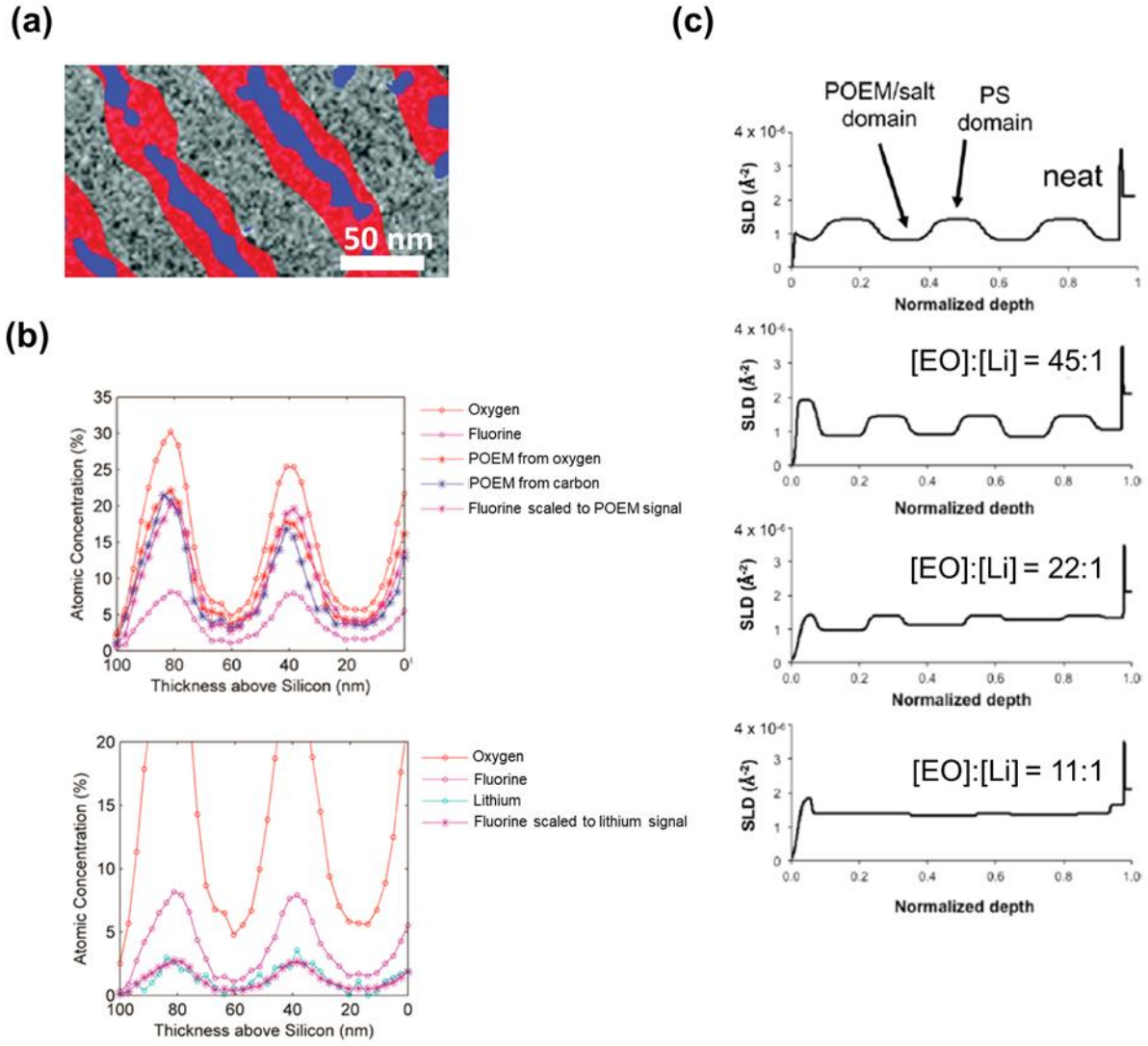

Fig. 7. The distribution of LiTFSI in BPs. (a) LiTFSI-doped PS-*b*-PEO measured by EFTEM with red regions representing PEO, blue regions representing lithium, and grey regions representing PS. Image was adapted with permission from ref. 95. Copyright 2009 American Chemical Society. (b) LiTFSI-doped PS-*b*-POEM measured by X-ray photoelectron spectroscopy depth profiling with C_{60}^+ sputtering. Atomic signals were scaled to depict the proportionality between POEM and LiTFSI signals. Images were adapted with permission from ref. 94 (https://pubs.acs.org/doi/abs/10.1021/nn505744r). Further permissions related to the material excerpted should be directed to the American Chemical Society. (c) LiTFSI-doped PS-*b*-POEM scattering length densities modeled from neutron reflectivity measurements. Normalized depth represents the distance into the film, with 0 representing the film-air interface and 1 representing the silicon substrate. Images were adapted with permission from ref. 89. Copyright 2018 American Chemical Society.

The segregation strength, in conjunction with the volumetric mesophase composition (*f*), dictates the self-assembled nanostructures formed by polymer electrolytes. Hexagonally packed cylinders, double gyroid (or other networks), and lamellae are of major interest for transport applications.[97] However, in minimally processed systems, these nanostructures exist in randomly-oriented grains that are ~1-7 times the domain size.[98, 99] Thus, transport through these nanostructures is dictated by their tortuosity on length scales smaller than grain size and by the connectivity of conducting pathways on length scales larger than the grain size.[100] Through effective medium theory, Sax and Ottino determined that the diffusion rates through randomly-oriented cylinders and lamellae were 0.33 and 0.67, respectively, of the diffusion rates in an equivalent homopolymer system.[101] These theoretical factors have been approached experimentally in high segregation strength PS-*b*-PEO systems (with a ~50 kg/mol PEO block and [Li]/[EO]~0.2), in which transport limitations due to poor solvation at the interface between the PS and PEO domains were negligible.[66, 99] The diffusion factors for a gyroid were 0.47-0.55 through the minority phase and 0.73-0.80 through the majority phase, as calculated through coarse-grained simulations, suggesting that such a bicontinuous network with an ion-conductive majority phase maximized ion transport.[102] Although network phases often are difficult to achieve in diblock copolymers,[103] triblock terpolymers[91, 104, 105] and tapered BPs[85, 106, 107] are among some alternative architectures that promote network stabilization.

The optimization of morphology can be aided by the availability of full polymer electrolyte phase diagrams, but the creation of such diagrams requires significant effort. Phase diagrams derived from experimental data are time-intensive due to the significant polymer synthesis requirements, parameter space of salt doping ratios and anion chemistries, and processing

protocols that must be surveyed for high-segregation-strength copolymers, whereas computational phase diagrams require deeper insight of ion and polymer interactions, as noted earlier. Current work is focused on computationally capturing the behavior of various systems through simple but accurate models. In one example, SCFT was extended to account for Coulombic interactions between ions (*via* liquid-state theory), and lithium ions were bound to the backbone of the high-dielectric polymer.[108] Unlike the phase diagram of a neat BP, the resulting phase diagram of the ion-doped polymer contained an asymmetric chimney-like regime that permitted phase separation at very low χN over a small compositional range, as shown in Fig. 8a.[108] This chimney-like regime was attributed to the Coulombic cohesion between ions, which led to strong ion aggregation within the high dielectric phase and decreased the tendency of mixing.[108] In separate work, Hou and Qin developed a different model with mobile ions that incorporated local dielectric heterogeneity, yet a similar phase diagram was reported (Fig. 8b); in this case, the chimney-like region resulted from the large energy required to move an ion between different dielectric media.[109] In contrast to these SCFT-based models, coarse-grained simulations by Chu et al. produced an asymmetric phase diagram with no chimney-like regime (Fig. 8c),[92] and this phase diagram showed qualitative agreement with a recently presented experimental phase diagram of LiTFSI-doped PS-*b*-PEO (Fig. 8d).[110] However, the experimental phase diagram contained small phase regions that were disconnected from larger regions of the same morphology.[110] Because these regions were not reported in the phase diagram of neat diblock copolymers such as PS-*b*-PI,[111] the small regions may be a feature of ion-containing systems. Further investigation of the origin of these small regions may provide insight into the appropriate thermodynamic models that can capture the unique features of ion-containing polymers.

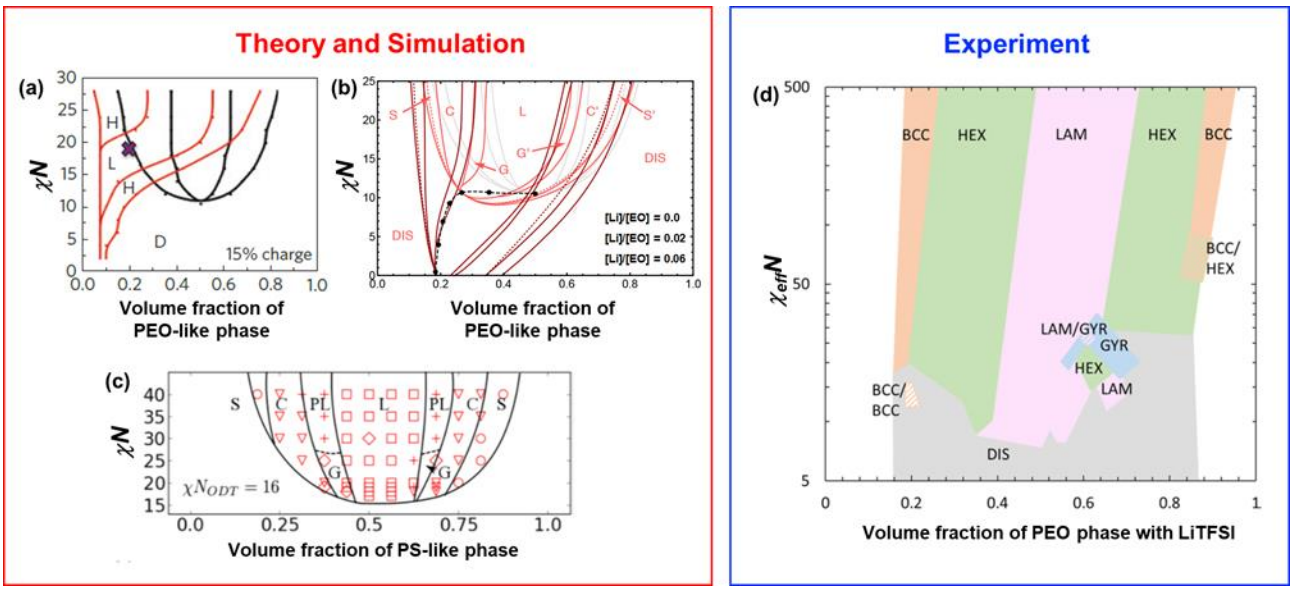

Fig. 8. Phase diagrams of salt-doped BPs. (a) SCFT in conjunction with liquid state theory of neutral diblock copolymers (black lines) and block copolyelectrolytes with 15% charge fraction (red lines). The purple cross represents a location in the disordered region that would transit into ordered phase through the addition of charge. Image was adapted by permission from Macmillan Publisher Ltd: Springer Nature Materials ref. 108, copyright 2014. (b) SCFT with local dielectric heterogeneity and Born solvation energy of salt-doped PS-*b*-PEO-like polymers. The black dashed line connects critical points at varying salt concentrations. Image was adapted with permission from ref. 109. Copyright 2018 American Chemical Society. (c) Coarse-grained simulations of salt-doped PS-*b*-PEO-like polymers in which salt doping decreased χN at the order-disorder transition from $(\chi N)_{ODT}$ = 18 to $(\chi N)_{ODT}$ = 16 and caused the phase diagram to shift toward the PS-rich side. Image was adapted with permission from ref. 92. Copyright 2017 American Chemical Society. (d) Experimental phase diagram of LiTFSI-doped PS-*b*-PEO at 100 °C. Image was adapted with permission from ref. 110. Copyright 2018 American Chemical Society.

Several advances in experimental and computational methodology can facilitate more accurate descriptions of polymer electrolyte thermodynamics, including the influence of local interactions and the establishment of long-range conductive pathways. The segregation strength can be manipulated to achieve optimal ion distributions; localized ion distributions are advantageous because the ions interact minimally with the low-conductivity interface, but may result in reduced chain dynamics in regions of higher local ion concentrations. Significant

knowledge can be gained if computational methods can capture the chemical details of monomer segments and ions to accurately predict the effective degree of segregation. On a local scale, ion distributions can be tuned selectively such that anion transport is suppressed, and lithium-ion transport is maximized (i.e., pseudo-single-ion materials). On a morphological scale, phase behavior can be mapped to effectively target desired nanostructures. On a size scale of multiple grains, the ability to model chemical details can be extended to additives, such as NPs, that can stabilize grain boundaries[112, 113] in a manner that promotes long-range pathways for ion transport. Thus, the thermodynamics of multicomponent electrolytes can be tailored to maximize lithium-ionic conductivity and simultaneously improve the robustness of LiBs.

5. Conclusions and Future Directions

Ion-conducting polymer electrolytes are an important component in safe, low-cost LiBs, but these materials require significant improvements in lithium-ionic conductivity to meet market demands. In this Perspective, we highlight how the integration of experimental and computational studies has expedited exploration of the key design parameters at scales from local ion and polymer interactions to the global thermodynamics of multicomponent electrolytes. At the smaller size scales, computational results were harnessed to rationalize local behavior, especially for cases in which the experimental characterization of that behavior was challenging. At the larger size scales, experimental results informed models to facilitate the incorporation of complex combinations of chemical components (e.g., chemistry, architecture, chain length, additive content) and macromolecular parameters (e.g., dielectric strength of local solvation sites, solvation site connectivity, monomer segment relaxation timescales, segregation strength, and mesophase composition). High-dielectric-strength solvation sites reduced the codiffusion of lithium ions with

other ionic species, and highly-connected solvation sites ensured that the free lithium ions had uninterrupted transport pathways through the conductive medium. Fast monomer segment relaxation promoted lithium-ion mobility *via* chain motion. The segregation strength influenced local ion solvation, chain mobility behavior, and large-scale self-assembly (along with the mesophase composition). The optimization of these parameters through novel polymer electrolyte designs will improve LiB performance.

Further advances in understanding the intra-electrolyte behavior highlighted above require experimental and computational tools to be expanded such that electrolyte materials can be screened and characterized more effectively. Experimental methods can be honed to characterize local ion solvation (and the nature of ion clusters) and segmental motion, that often are predicted *via* computational means. Although the experimental quantification of ion clusters through a single technique is difficult, a combination of multiple tools to measure the types of interactions between individual ions (e.g., Raman and infrared spectroscopy), the amount of mobile free cations and anions (e.g., electrochemical impedance spectroscopy), and the amount of various mobile ion clusters (e.g., solid-state nuclear magnetic resonance spectroscopy) may elucidate the size and compositional profile of the ion clusters.[71] The local chain dynamics, which can be gauged through the application of dynamic mechanical analysis, amplitude-modulated atomic force microscopy, solid state nuclear magnetic resonance spectroscopy, or fluorescence measurements of marker monomers,[68-70] may provide a more comprehensive determination of ion mobility than global T_g or relaxation timescale measurements. These quantifications of ion solvation and chain dynamics can be connected to the rate and direction of ion migration, *via* Stefan-Maxwell diffusion coefficients,[114, 115] to understand the effects of architectural features, such as chemical junctions in BPs, crosslinks, and branch points, on ion transport.[116-118] These behaviors also can be

characterized in a realistic battery environment through the formulation of *in operando* tools to probe morphology,[119] dielectric interactions (*via* Raman or infrared spectroscopy), etc. Pedagogical resources for computational methods, such as open source software and a guide by Arora et al. to perform SCFT calculations on a desktop computer,[120] will encourage more experimentalists to incorporate computational insights into their efforts to enhance experimental designs.

Computational tools can be augmented by including the numerous features of charged systems such as charge dissociation, dielectric inhomogeneity, and chemistry of the anions. The ability to capture these details then can be extended to other additive species such as ILs and NPs to translate both local interactions and larger-scale thermodynamic behavior to experimental conditions. One area that is ripe for further advances is the computational analysis of ionic conductivity and transference number. Although the calculation of ion self-diffusion constants from molecular simulations and experiments is straightforward, the ionic conductivity is more difficult to calculate accurately because the effects of self-diffusion and the degree of cation/anion codiffusion are coupled. The degree of ion codiffusion has been explicitly calculated in equilibrium simulations,[41, 121] but the application of an external electric field to analyze ionic mobility in non-equilibrium conditions may provide improved statistics.[122, 123] Not only can calculated ionic conductivities be compared to experimental measurements, but transference number calculations may complement the challenging experimental measurements.[44] Innovations in this area would elucidate the mechanisms that contribute to lithium-ion transport, and these models can be capitalized to rapidly screen favorable polymer electrolyte designs to guide synthetic efforts. In one such example, all-atom and coarse-grained MD simulations were combined to understand and optimize ion conduction in polymerized ILs.[124] Other classes of

conductive macromolecules, in which similar models can be leveraged, include single-ion polymers with enhanced ion solvation, pseudo-single-ion materials with various mechanisms for anion sequestration, and electrolytes with decoupled lithium-ion solvation and segmental motion behavior. In particular, the manipulation of end-group chemistry can sequester anions through dielectric means or facilitate non-covalent chain tethers to modulate chain dynamics.[57] The establishment of meaningful collaborations between computational and experimental researchers can enable rapid validation of these new approaches, because experimental systems can be designed to readily translate to computational analogues. Several examples of such collaborations were highlighted in this Perspective, and continued collaborative efforts will accelerate the development of viable electrolytes.

The integration of polymer electrolytes into LiBs necessitates that intra-electrolyte behavior be linked to interactions between the electrodes and electrolyte. Safety-related phenomena (e.g., electrochemical instability and lithium dendrite formation) and the consequent performance-related concerns (e.g., reduced LiB lifetime, capacity loss, and electrolyte delamination) often have been associated with undesirable interactions at the electrode-electrolyte interface.[7, 78] Although lithium dendrites are believed to nucleate within the electrode,[125] several characteristics of the electrolyte can mitigate the negative impact of these protrusions. For example, dendrites have been impeded mechanically with high-modulus and high-thickness electroytes,[126, 127] and the nature of lithium electrodeposition has been manipulated through the control of the current density passed across the electrode-electrolyte interface.[128, 129] Both high modulus and control of charge polarization have been exemplified in single-ion polymers, but these attributes were not universally present in all dendrite-resistant materials (e.g., cross-linked electrolytes).[16, 89, 130] Deeper insight into the multitude of mechanisms that occur at the

electrode-electrolyte interface[7, 131] and the deconvolution of the effects of mechanical and electrochemical dendrite-resistance pathways[16] can inform how various electrolytes retain stability. However, it is challenging to probe these mechanisms with typical experiments or simulations because the rich chemistry and physics at the electrode-electrolyte interface involves multiple length scales. The electrochemical reactions that occur at the electrode-electrolyte interface can be examined in isolation if conditions at which those respective reactions are rate-limiting can be achieved, and these conditions were suggested by Hallinan et al..[132] DFT calculations and *ab initio* MD simulations can be leveraged to further deconvolute reactions that cannot be isolated easily through experiment.[133-135] The dendrite growth that results from these reactions can be studied through *post-mortem* analyses of cycled cells[125, 126] or through *in operando* magnetic resonance imaging,[136] and these results can guide the development of multiphysics models[127, 129, 136] to quantify deposition behavior.

In summary, fundamental knowledge of the design challenges for polymer electrolytes, and physical parameters associated with each challenge, is crucial to advance the development of polymer electrolyte systems that can enhance battery performance and eliminate safety concerns. Such knowledge can be achieved through the synergistic combination of experimental and computational efforts. We discussed recent efforts in the areas of local ion and polymer interactions, chain dynamics, and polymer thermodynamics that have furthered the understanding of certain universal parameters. Future directions involve the augmentation of current methods to connect experimental and computational insights more closely and to apply these tools to realize next-generation materials. The development of efficient methods that unite the breadth of polymer electrolyte designs under current investigation will accelerate the market penetration of safer and lower-cost LiBs.

Conflicts of interest

There are no conflicts of interest to declare.

Acknowledgements

P.M.K., K.-H.S., L.M.H., and T.H.E. gratefully acknowledge the United States Department of Energy Basic Energy Sciences (DE-SC0014458), and P.M.K. and T.H.E. thank Samsung (17A01588) for financial support during the writing of this manuscript. T.H.E. acknowledges the financial support from the Thomas & Kipp Gutshall Professorship.

References

1. *Lithium-ion battery - global market outlook (2017-2026)*, 2018.
2. A. Chatzivasileiadi, E. Ampatzi and W. I. Knight, *Renewable and Sustainable Energy Reviews*, 2013, **25**, 814-830.
3. M. Armand and J. M. Tarascon, *Nature*, 2008, **451**, 652-657.
4. S. Choi and G. X. Wang, *Advanced Materials Technologies*, 2018, **3**.
5. T. Tao, S. G. Lu and Y. Chen, *Advanced Materials Technologies*, 2018, **3**.
6. H. Cha, J. Kim, Y. Lee, J. Cho and M. Park, *Small*, 2018, **14**.
7. B. Scrosati and J. Garche, *Journal of Power Sources*, 2010, **195**, 2419–2430.
8. S. S. Zhang, *Journal of Power Sources*, 2007, **164**, 351–364.
9. P. Arora and Z. Zhang, *Chemical Reviews*, 2004, **104**, 4419−4462.
10. S. Manzetti and F. Mariasiu, *Renewable and Sustainable Energy Reviews*, 2015, **51**, 1004–1012.
11. K. Xu, *Chemical Reviews*, 2004, **104**, 4303-4417.
12. F. Zheng, M. Kotobuki, S. F. Song, M. O. Lai and L. Lu, *Journal of Power Sources*, 2018, **389**, 198-213.
13. M. B. Armand, *Annual Review of Materials Science*, 1986, **16**, 245-261.
14. W. H. Meyer, *Advanced Materials*, 1998, **10**, 439-448.
15. A. Arya and A. L. Sharma, *Ionics*, 2017, **23**, 497-540.
16. M. A. Morris, H. An, J. L. Lutkenhaus and T. H. Epps, III, *ACS Energy Letters*, 2017, **2**, 1919-1936.
17. E. Quartarone, P. Mustarelli and A. Magistris, *Solid State Ionics*, 1998, **110**, 1-14.
18. W.-S. Young, W.-F. Kuan and T. H. Epps, III, *Journal of Polymer Science, Part B: Polymer Physics*, 2014, **52**, 1-16.

19. M. A. Morris, T. E. Gartner and T. H. Epps, III, *Macromolecular Chemistry and Physics*, 2017, **218**, 1600513.
20. W.-F. Kuan, R. Remy, M. E. Mackay and T. H. Epps, III, *RSC Advances*, 2015, **5**, 12597-12604.
21. C. M. Bates, A. B. Chang, N. Momčilović, S. C. Jones and R. H. Grubbs, *Macromolecules*, 2015, **48**, 4967-4973.
22. G. Zardalidis, A. Pipertzis, G. Mountrichas, S. Pispas, M. Mezger and G. Floudas, *Macromolecules*, 2016, **49**, 2679-2687.
23. T. Niitani, M. Amaike, H. Nakano, K. Dokko and K. Kanamura, *Journal of The Electrochemical Society*, 2009, **156**, A577.
24. D. Lee, H. Y. Jung and M. J. Park, *ACS Macro Letters*, 2018, **7**, 1046-1050.
25. R. Khurana, J. L. Schaefer, L. A. Archer and G. W. Coates, *Journal of the American Chemical Society*, 2014, **136**, 7395-7402.
26. L. D. McIntosh, T. Kubo and T. P. Lodge, *Macromolecules*, 2014, **47**, 1090-1098.
27. S. K. Fullerton-Shirey and J. K. Maranas, *Journal of Physical Chemistry C*, 2010, **114**, 9196-9206.
28. W. Wang and P. Alexandridis, *Polymers*, 2016, **8**.
29. Y.-S. Ye, J. Rick and B.-J. Hwang, *Journal of Materials Chemistry A*, 2013, **1**, 2719-2743.
30. I. Osada, H. de Vries, B. Scrosati and S. Passerini, *Angewandte Chemie-International Edition*, 2016, **55**, 500-513.
31. Z. Wen, T. Itoh, Y. Ichikawa, M. Kubo and O. Masataka, *Solid State Ionics*, 2000, **134**, 281–289.
32. R. Arunkumar, R. S. Babu, M. U. Rani and S. Kalainathan, *Journal of Applied Polymer Science*, 2017, **44939**, 1-12.
33. M. Zhao, X. Zuo, X. Ma, X. Xiao, J. Liu and J. Nan, *Journal of Membrane Science*, 2017, **532**, 30-37.
34. T. E. Gartner, T. Kubo, Y. Seo, M. Tansky, L. M. Hall, B. S. Sumerlin and T. H. Epps, III, *Macromolecules*, 2017, **50**, 7169-7176.
35. S. Mogurampelly, O. Borodin and V. Ganesan, *Annual Review of Chemical and Biomolecular Engineering*, 2016, **7**, 349-371.
36. D. Diddens and A. Heuer, *ACS Macro Letters*, 2013, **2**, 322-326.
37. O. Borodin, in *Electrolytes for lithium and lithium-ion batteries*, Springer, New York, NY, 2014, vol. 58, ch. Molecular modeling of electrolytes, pp. 371-401.
38. S. Mogurampelly, J. R. Keith and V. Ganesan, *Journal of the American Chemical Society*, 2017, **139**, 9511-9514.
39. V. Sethuraman, S. Mogurampelly and V. Ganesan, *Macromolecules*, 2017, **50**, 4542-4554.
40. M. A. Webb, B. M. Savoie, Z. G. Wang and T. F. Miller, *Macromolecules*, 2015, **48**, 7346-7358.
41. B. K. Wheatle, N. A. Lynd and V. Ganesan, *ACS Macro Letters*, 2018, **7**, 1149-1154.
42. D. M. Pesko, M. A. Webb, Y. Jung, Q. Zheng, T. F. Miller, III, G. W. Coates and N. P. Balsara, *Macromolecules*, 2016, **49**, 5244-5255.
43. B. K. Wheatle, J. R. Keith, S. Mogurampelly, N. A. Lynd and V. Ganesan, *ACS Macro Letters*, 2017, **6**, 1362-1367.
44. K. M. Diederichsen, E. J. McShane and B. D. McCloskey, *ACS Energy Letters*, 2017, **2**, 2563-2575.

45. E. W. Stacy, C. P. Gainaru, M. Gobet, Z. Wojnarowska, V. Bocharova, S. G. Greenbaum and A. P. Sokolov, *Macromolecules*, 2018, **51**, 8637-8645.
46. C. T. Elmore, M. E. Seidler, H. O. Ford, L. C. Merrill, S. P. Upadhyay, W. F. Schneider and J. L. Schaefer, *Batteries*, 2018, **4**, 1-17.
47. N. Molinari, J. P. Mailoa and B. Kozinsky, *Chemistry of Materials*, 2018, **30**, 6298-6306.
48. M. M. Doeff, P. Georen, J. Qiao, J. Kerr and L. C. De Jonghe, *Journal of the Electrochemical Society*, 1999, **146**, 2024-2028.
49. A. Ferry, M. M. Doeff and L. C. De Jonghe, *Journal of the Electrochemical Society*, 1998, **145**, 1586-1592.
50. A. Ferry, M. M. Doeff and L. C. DeJonghe, *Electrochimica Acta*, 1998, **43**, 1387-1393.
51. Y. P. Ma, M. Doyle, T. F. Fuller, M. M. Doeff, L. C. Dejonghe and J. Newman, *Journal of the Electrochemical Society*, 1995, **142**, 1859-1868.
52. F. Müller-Plathe and W. F. Van Gunsteren, *The Journal of Chemical Physics*, 1995, **103**.
53. M. A. Webb, Y. Jung, D. M. Pesko, B. M. Savoie, U. Yamamoto, G. W. Coates, N. P. Balsara, Z.-G. Wang and T. F. Miller, III, *ACS Central Science*, 2015, **1**, 198-205.
54. Q. Zheng, D. M. Pesko, B. M. Savoie, K. Timachova, A. L. Hasan, M. C. Smith, T. F. Miller, III, G. W. Coates and N. P. Balsara, *Macromolecules*, 2018, **51**, 2847-2858.
55. B. M. Savoie, M. A. Webb and T. F. Miller, *Journal of Physical Chemistry Letters*, 2017, **8**, 641-646.
56. V. Ganesan, V. Pyramitsyn, C. Bertoni and M. Shah, *ACS Macro Letters*, 2012, **1**, 513-518.
57. H. Y. Jung, P. Mandal, G. Jo, O. Kim, M. Kim, K. Kwak and M. J. Park, *Macromolecules*, 2017, **50**, 3224-3233.
58. K. Sinha and J. Maranas, *Macromolecules*, 2014, **47**, 2718-2726.
59. D. Fragiadakis, S. Dou, R. H. Colby and J. Runt, *The Journal of Chemical Physics*, 2009, **130**, 064907.
60. W. Wang, W. Liu, G. J. Tudryn, R. H. Colby and K. I. Winey, *Macromolecules*, 2010, **43**, 4223-4229.
61. K. J. Lin and J. K. Maranas, *Physical Review E*, 2013, **88**, 052602.
62. K. I. S. Mongcopa, M. Tyagi, J. P. Mailoa, G. Samsonidze, B. Kozinsky, S. A. Mullin, D. A. Gribble, H. Watanabe and N. P. Balsara, *ACS Macro Letters*, 2018, **7**, 504-508.
63. I. Nakamura, N. P. Balsara and Z.-G. Wang, *Physical Review Letters*, 2011, **107**, 198301(198301-198305).
64. M. A. Webb, U. Yamamoto, B. M. Savoie, Z. G. Wang and T. F. Miller, *ACS Macro Letters*, 2018, **7**, 734-738.
65. J. Shi and C. A. Vincent, *Solid State Ionics*, 1993, **60**, 11-17.
66. A. Panday, S. Mullin, E. D. Gomez, N. Wanakule, V. L. Chen, A. Hexemer, J. Pople and N. P. Balsara, *Macromolecules*, 2009, **42**, 4632-4637.
67. V. Sethuraman, V. Pryamitsyn and V. Ganesan, *Journal of Polymer Science, Part B: Polymer Physics*, 2016, **54**, 859-864.
68. H. K. Nguyen, X. Liang, M. Ito and K. Nakajima, *Macromolecules*, 2018, **51**, 6085-6091.
69. H. Schneider, K. Saalwächter and M. Roos, *Macromolecules*, 2017, **50**, 8598-8610.
70. D. Christie, R. A. Register and R. D. Priestley, *ACS Central Science*, 2018, **4**, 504-511.
71. M. Joost, M. Kunze, S. Jeong, M. Schonhoff, M. Winter and S. Passerini, *Electrochimica Acta*, 2012, **86**, 330-338.

72. J. H. Ahn, G. X. Wang, H. K. Liu and S. X. Dou, *Journal of Power Sources*, 2003, **119-121**, 422-426.
73. L. V. N. R. Ganapatibhotla and J. K. Maranas, *Macromolecules*, 2014, **47**, 3625-3634.
74. S. Mogurampelly and V. Ganesan, *Macromolecules*, 2015, **48**, 2773-2786.
75. O. Borodin, G. D. Smith, R. Bandyopadhyaya, P. Redfern and L. A. Curtiss, *Modelling and Simulation in Materials Science and Engineering*, 2004, **12**, S73-S89.
76. S. Wang, X. Liu, A. L. Wang, Z. N. Wang, J. Chen, Q. H. Zeng, X. F. Wang and L. Y. Zhang, *Polymer Chemistry*, 2018, **9**, 4674-4682.
77. O. Durr, W. Dieterich and A. Nitzan, *Journal of Chemical Physics*, 2004, **121**, 12732-12739.
78. L. P. Yue, J. Ma, J. J. Zhang, J. W. Zhao, S. M. Dong, Z. H. Liu, G. L. Cui and L. Q. Chen, *Energy Storage Materials*, 2016, **5**, 139-164.
79. M. W. Matsen and M. Schick, *Physical Review Letters*, 1994, **72**, 2660-2663.
80. G. H. Fredrickson and F. S. Bates, *Annual Review Of Materials Science*, 1996, **26**, 501-550.
81. F. S. Bates and G. H. Fredrickson, *Annual Review of Physical Chemistry*, 1990, **41**, 525-557.
82. M. W. Matsen and F. S. Bates, *Macromolecules*, 1996, **29**, 1091-1098.
83. A. B. Chang, C. M. Bates, B. Lee, C. M. Garland, S. C. Jones, R. K. W. Spencer, M. W. Matsen and R. H. Grubbs, *Proceedings of the National Academy of Sciences of the United States of America*, 2017, **114**, 6462-6467.
84. D. F. Sunday, A. B. Chang, C. D. Liman, E. Gann, D. M. Delongchamp, L. Thomsen, M. W. Matsen, R. H. Grubbs and C. L. Soles, *Macromolecules*, 2018, **51**, 7178-7185.
85. W.-F. Kuan, E. H. Reed, N. A. Nguyen, M. E. Mackay and T. H. Epps, III, *MRS Communications*, 2015, **5**, 251-256.
86. P. Medapuram, J. Glaser and D. C. Morse, *Macromolecules*, 2015, **48**, 819-839.
87. J. Glaser, J. Qin, P. Medapuram and D. C. Morse, *Macromolecules*, 2014, **47**, 851-869.
88. W. Zhang, E. D. Gomez and S. T. Milner, *Physical Review Letters*, 2017, **119**, 017801.
89. T. E. Gartner, III, M. Morris, A., C. K. Shelton, J. Dura, A. and T. H. Epps, III, *Macromolecules*, 2018, **51**, 1917-1926.
90. W. S. Young and T. H. Epps, III, *Macromolecules*, 2009, **42**, 2672-2678.
91. T. H. Epps, III, T. S. Bailey, R. Waletzko and F. S. Bates, *Macromolecules*, 2003, **36**, 2873-2881.
92. W. Chu, J. Qin and J. J. de Pablo, *Macromolecules*, 2018, **51**, 1986-1991.
93. J. R. Brown, Y. Seo and L. M. Hall, *Physical Review Letters*, 2018, **120**, 127801.
94. J. B. Gilbert, M. Luo, C. K. Shelton, M. F. Rubner, R. E. Cohen and T. H. Epps, III, *ACS Nano*, 2015, **9**, 512-520.
95. E. D. Gomez, A. Panday, E. H. Feng, V. Chen, G. M. Stone, A. M. Minor, C. Kisielowski, K. H. Downing, O. Borodin, G. D. Smith and N. P. Balsara, *Nano Letters*, 2009, **9**, 1212–1216.
96. W.-S. Young and T. H. Epps, *Macromolecules*, 2009, **42**, 2672-2678.
97. C. X. Zhai, H. H. Zhou, T. Gao, L. L. Zhao and S. C. Lin, *Macromolecules*, 2018, **51**, 4471-4483.
98. O. Oparaji, S. Narayanan, A. Sandy, S. Ramakrishnan and D. Hallinan, *Macromolecules*, 2018, **51**, 2591-2603.

99. M. Chintapalli, T. N. P. Le, N. R. Venkatesan, N. G. Mackay, A. A. Rojas, J. L. Thelen, X. C. Chen, D. Devaux and N. P. Balsara, *Macromolecules*, 2016, **49**, 1770-1780.
100. C. G. Arges, Y. Kambe, M. Dolejsi, G.-P. Wu, T. Segal-Pertz, J. Ren, C. Cao, G. S. W. Craig and P. F. Nealey, *Journal of Materials Chemistry A*, 2017, **5**, 5619-5629.
101. J. Sax and J. M. Ottino, *Polymer Engineering and Science*, 1983, **23**, 165-176.
102. K.-H. Shen, J. R. Brown and L. M. Hall, *ACS Macro Letters*, 2018, **7**, 1092-1098.
103. M. W. Matsen, *Macromolecules*, 2012, **45**, 2161-2165.
104. A. J. Meuler, M. A. Hillmyer and F. S. Bates, *Macromolecules*, 2009, **42**, 7221-7250.
105. E. W. Cochran, D. C. Morse and F. S. Bates, *Macromolecules*, 2003, **36**, 782-792.
106. J. R. Brown, S. W. Sides and L. M. Hall, *ACS Macro Letters*, 2013, **2**, 1105-1109.
107. W. F. Kuan, R. Roy, L. X. Rong, B. S. Hsiao and T. H. Epps, *ACS Macro Letters*, 2012, **1**, 519-523.
108. C. E. Sing, J. W. Zwanikken and M. O. de la Cruz, *Nature Materials*, 2014, **13**, 694-698.
109. K. J. Hou and J. Qin, *Macromolecules*, 2018, **51**, 7463-7475.
110. W. S. Loo, M. D. Galluzzo, X. Li, J. A. Maslyn, H. J. Oh, K. I. Mongcopa, C. Zhu, A. A. Wang, X. Wang, B. A. Garetz and N. P. Balsara, *The Journal of Physical Chemistry*, 2018, **122**, 8065-8074.
111. A. K. Khandpur, S. Forster, F. S. Bates, I. W. Hamley, A. J. Ryan, W. Bras, K. Almdal and K. Mortensen, *Macromolecules*, 1995, **28**, 8796-8806.
112. H. J. Ryu, J. Sun, A. Avgeropoulos and M. R. Bockstaller, *Macromolecules*, 2014, **47**, 1419-1427.
113. J. S. Smith, D. Bedrov and G. D. Smith, *Composites Science and Technology*, 2003, **63**, 1599-1605.
114. J. Newman and K. E. Thomas-Alyea, *Electrochemical Systems*, John Wiley & Sons, Inc., Hoboken, New Jersey, 3 edn., 2004.
115. M. Doyle and J. Newman, *Journal of the Electrochemical Society*, 1995, **142**, 3465-3468.
116. E. Senses, M. Tyagi, M. Pasco and A. Faraone, *ACS Nano*, 2018, **12**, 10807-10816.
117. Y. Shibuya, R. Tatara, Y. Jiang, Y. Shao-Horn and J. Johnson, *Journal of Polymer Science, Part A: Polymer Chemistry*, 2018.
118. L. Liu, W. K. den Otter and W. J. Briels, *The Journal of Physical Chemistry B*, 2018, **122**, 10210-10218.
119. G. E. Mohl, E. Metwalli and P. Muller-Buschbaum, *ACS Energy Letters*, 2018, **3**, 1525-1530.
120. A. Arora, J. Qin, D. C. Morse, K. T. Delaney, G. H. Fredrickson, F. S. Bates and K. D. Dorfman, *Macromolecules*, 2016, **49**, 4675-4690.
121. O. Borodin and G. D. Smith, *Macromolecules*, 2006, **39**, 1620-1629.
122. C. L. Ting, M. J. Stevens and A. Frischknecht, *Macromolecules*, 2015, **48**, 809-818.
123. M. S. Alshammasi and F. A. Escobedo, *Macromolecules*, 2018, **51**.
124. Y. Z. Cheng, J. H. Yang, J. H. Hung, T. K. Patra and D. S. Simmons, *Macromolecules*, 2018, **51**, 6630-6644.
125. K. J. Harry, D. T. Hallinan, D. Y. Parkinson, A. A. MacDowell and N. P. Balsara, *Nature Materials*, 2014, **13**, 69-73.
126. D. T. Hallinan, S. A. Mullin, G. M. Stone and N. P. Balsara, *Journal of the Electrochemical Society*, 2013, **160**, A464-A470.
127. C. Monroe and J. Newman, *Journal of the Electrochemical Society*, 2005, **152**, A396-A404.

128. J. A. Maslyn, W. S. Loo, K. D. McEntush, H. J. Oh, K. J. Harry, D. Y. Parkinson and N. P. Balsara, *The Journal of Physical Chemistry C*, 2018, **122**.
129. P. Barai, K. Higa and V. Srinivasan, *Physical Chemistry Chemical Physics*, 2017, **19**, 20493-20505.
130. R. Bouchet, S. Maria, R. Meziane, A. Aboulaich, L. Lienafa, J. P. Bonnet, T. N. T. Phan, D. Bertin, D. Gigmes, D. Devaux, R. Denoyel and M. Armand, *Nature Materials*, 2013, **12**, 452-457.
131. M. D. Tikekar, S. Choudhury, Z. Y. Tu and L. A. Archer, *Nature Energy*, 2016, **1**, 1-7.
132. D. T. Hallinan, Jr., I. Villaluega and N. P. Balsara, *MRS Bulletin*, 2018, **43**, 759-767.
133. F. A. Soto, A. Marzouk, F. El-Mellouhi and P. B. Balbuena, *Chemistry of Materials*, 2018, **30**, 3315-3322.
134. Y. Ozhabes, D. Gunceler and T. A. Arias, *Stability and surface diffusion at lithium-electrolyte interphases with connections to dendrite suppression*, Report **arXiv:1504.05799 [cond-mat.mtrl-sci]**, Cornell University, 2015.
135. S. Choudhury, S. Y. Wei, Y. Ozhabes, D. Gunceler, M. J. Zachman, Z. Y. Tu, J. H. Shin, P. Nath, A. Agrawal, L. F. Kourkoutis, T. A. Arias and L. A. Archer, *Nature Communications*, 2017, **8**.
136. A. J. Ilott, M. Mohammadi, H. J. Chang, C. P. Grey and A. Jerschow, *Proceedings of the National Academy of Sciences of the United States of America*, 2016, **113**, 10779-10784.

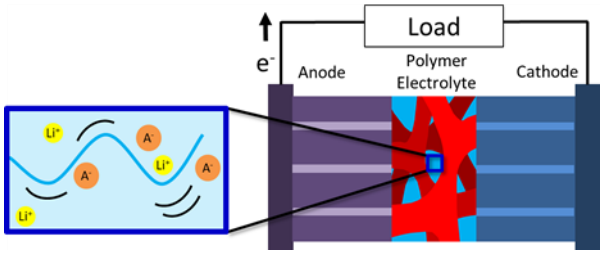

TOC Figure. Lithium-ion battery performance is governed by ionic transport mechanisms over a wide range of size scales